

# Turbulence decay in the density-stratified intracluster medium

Xun Shi<sup>1,2\*</sup>, Congyao Zhang<sup>2</sup>

<sup>1</sup>South-Western Institute for Astronomy Research (SWIFAR), Yunnan University, 650500 Kunming, P. R. China

<sup>2</sup>Max-Planck-Institut für Astrophysik (MPA), Karl-Schwarzschild-Straße 1, D-85740 Garching bei München, Germany

17 March 2022

## ABSTRACT

Turbulence evolution in a density-stratified medium differs from that of homogeneous isotropic turbulence described by the Kolmogorov picture. We evaluate the degree of this effect in the intracluster medium (ICM) with hydrodynamical simulations. We find that the buoyancy effect induced by ICM density stratification introduces qualitative changes to the turbulence energy evolution, morphology, and the density fluctuation - turbulence Mach number relation, and likely explains the radial dependence of the ICM turbulence amplitude as found previously in cosmological simulations. A new channel of energy flow between the kinetic and the potential energy is opened up by buoyancy. When the gravitational potential is kept constant with time, this energy flow leaves oscillations to the energy evolution, and leads to a balanced state of the two energies where both asymptote to power-law time evolution with slopes shallower than that for the turbulence kinetic energy of homogeneous isotropic turbulence. We discuss that the energy evolution can differ more significantly from that of homogeneous isotropic turbulence when there is a time variation of the gravitational potential. Morphologically, ICM turbulence can show a layered vertical structure and large horizontal vortical eddies in the central regions with the greatest density stratification. In addition, we find that the coefficient in the linear density fluctuation - turbulence Mach number relation caused by density stratification is in general a variable with position and time.

**Key words:** cosmology: theory – galaxies: clusters: intracluster medium – turbulence – methods: numerical

## 1 INTRODUCTION

According to our current knowledge of cosmic structure formation, galaxy clusters are the largest virialized objects on the top of the structure growth hierarchy in our Universe today. They form via merging and accretion of smaller units of matter, which would generate turbulent motions in their reservoir of diffuse hot gas – the intracluster medium (ICM), as demonstrated by hydrodynamic numerical simulations (e.g. Norman & Bryan 1999; Iapichino & Niemeyer 2008; Nelson et al. 2012). Some recent dedicated simulations have investigated the statistical properties of the turbulent motions in the ICM, mainly their compressibility and spectral properties (e.g. Miniati 2014; Miniati & Beresnyak 2015; Vazza et al. 2009, 2017).

Observationally, the ubiquitous of turbulence in the ICM is confirmed by a direct detection of the non-thermal broadening of the X-ray emission lines by the *Hitomi* satellite (Hitomi Collaboration et al. 2016), as well as indirect observations of the magnetic field fluctuations in the diffuse cluster radio sources (Murgia et al. 2004; Vogt & Enßlin 2005; Bonafede et al. 2010; Vacca et al. 2010, 2012), X-ray surface brightness fluctuations or pressure fluctuations inferred from X-ray maps and Sunyaev-Zel’dovich effect

maps (Schuecker et al. 2004; Churazov et al. 2012; Walker et al. 2015; Khatri & Gaspari 2016; Zhuravleva et al. 2018), and the suppression of resonant line scattering in the X-ray spectra (Churazov et al. 2004; Zhuravleva et al. 2013; Hitomi Collaboration et al. 2018). In the near future, direct measurements of ICM turbulence will reach an unprecedented sensitivity thanks to the planned *XRISM* and *Athena* satellites (see Simionescu et al. 2019 for a recent review).

The theoretical framework that is widely used for turbulence studies is the idealized Kolmogorov picture of homogeneous and isotropic turbulence. However, the ICM is neither homogeneous nor isotropic, it is in rough hydrostatic equilibrium with the gravitational field that bounds it, and as a consequence, its density is radial-dependent i.e. stratified. If and how would this density stratification influence ICM turbulence is the topic of this study.

In previous numerical studies of ICM gas motions, there are hints of a radial dependence that is neglected by the Kolmogorov picture. Studies of cluster samples in cosmological hydrodynamical simulations have discovered a slightly increasing amplitude of non-thermal ICM gas motions with cluster radius despite that the thermal velocity a.k.a. sound speed decreases with radius (Lau et al. 2009; Battaglia et al. 2012; Nelson et al. 2014; Shi et al. 2015). In the analytical model of the ICM non-thermal pressure by Shi & Komatsu (2014), a radial-dependent turbulence dissipation time is

\* E-mail: xun@ynu.edu.cn

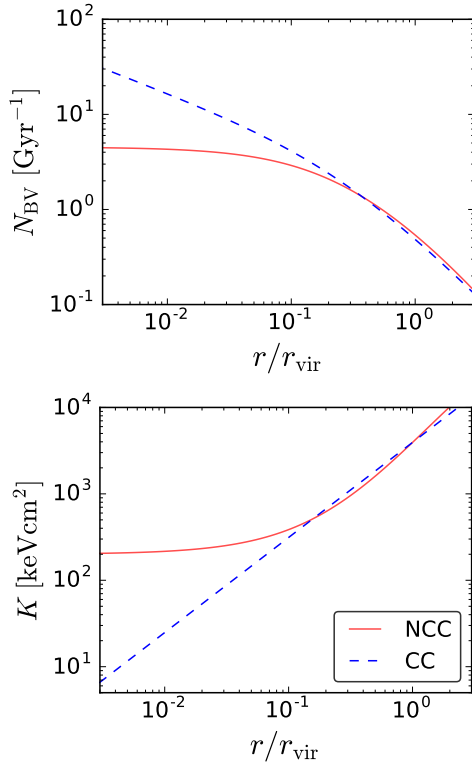


**Figure 1.** Typical profiles of the Brunt-Väisälä frequency (Eq. 1) in the ICM for cool-core (CC) and non-cool-core (NCC) clusters (top panel) and the corresponding entropy profiles (bottom panel). The NCC profiles are modelled with the Komatsu & Seljak (2001) analytical model for a  $10^{15} M_{\odot}$  cluster at redshift zero. The CC profiles use the same NFW mass profile (Navarro et al. 1996) as the NCC model, together with a typical entropy profile for a cool-core cluster,  $K \propto r^{1.1}$ .

responsible for this radial dependence. The success of this analytical model (Shi et al. 2015, 2016) motivated Shi et al. (2018) to verify this ansatz by performing a detailed multi-scale analysis of ICM turbulence evolution in cosmological hydrodynamical simulations, where they found clear evidence of faster turbulence dissipation in the central regions compared to the outer regions of the ICM after injection at a major merger. In this paper, we continue to explore the physical mechanism underlying such radial dependent turbulence decay by investigating the effect of ICM density stratification. We will introduce the physics of turbulence evolution in a density-stratified medium in Sect. 2, describe our simulation design in Sect. 3, and present our results in Sect. 4. Then we will discuss some physics neglected in this study in Sect. 5 and conclude in Sect. 6.

## 2 PHYSICS OF TURBULENCE EVOLUTION IN A DENSITY-STRATIFIED MEDIUM

Turbulence evolution in a density-stratified system has been studied since long in ocean and atmosphere sciences (e.g. Ozmidov 1965; Stillinger et al. 1983; Hopfinger 1987).

In a density-stratified system such as the ICM, gas motions lead inevitably to density fluctuations. Also due to density stratification, the density fluctuations are subject to a buoyancy force, which in turn alters the velocity field. In other words, there exists a fundamental difference between turbulence in a stably density-

stratified medium and its homogeneous counterpart – the presence of restoring forces in the vertical direction.

The buoyancy restoring force introduces a new time scale to the system, which is characterized by the Brunt-Väisälä frequency

$$N_{\text{BV}} = \sqrt{-\frac{g}{\gamma} \frac{d \ln K}{dr}}, \quad (1)$$

which is determined by the amplitude of the background gravitational acceleration  $g$  and the entropy profile  $K(r)$  of the galaxy cluster. Here  $\gamma$  is the adiabatic index of the ICM. As shown by Fig. 1, the Brunt-Väisälä frequency differs by an order of magnitude from the cluster center to the virial radius for a typical non-cool-core cluster, and even more for a typical cool-core cluster which has a steep  $N_{\text{BV}}$  profile in its core region<sup>1</sup>.

The important parameter describing the relative strength of the buoyancy force compared to the inertia of the turbulence is the Froude number

$$Fr = \frac{\sigma}{N_{\text{BV}} \ell_g} \quad (2)$$

where  $\sigma$  is the turbulence velocity dispersion and

$$\ell_g = \frac{\int k^{-1} E(k) dk}{\int E(k) dk} \quad (3)$$

is a lateral integral scale of the turbulence energy spectrum  $E(k)$ , with  $2\pi\ell_g$  characterizing the energy-containing scale<sup>2</sup>. The Froude number describes the ratio of the buoyancy and the typical turbulence eddy turn-over time scales. Generally speaking,  $Fr < O(1)$  (buoyancy time  $\lesssim$  turbulence eddy turn-over time) suggests that the buoyancy force becomes dynamically important, whereas  $Fr \gg 1$  (buoyancy time  $\gg$  turbulence eddy turn-over time) suggests homogeneous isotropic turbulence unaffected by density stratification (e.g. Riley & deBruynKops 2003).

Apart from  $\ell_g$ , another fundamental turbulence length scale associated with density stratification is the buoyancy scale

$$L_b = \frac{2\pi\sigma}{N_{\text{BV}}}, \quad (4)$$

which characterizes the thickness of the shear layers in stratified turbulence. One can see that the Froude number also reflects the ratio of the two length scales  $Fr \propto L_b/\ell_g$ .

Turbulence under the influence of an extreme density stratification ( $Fr \ll 1$ ) is morphologically resemblant to 2D turbulence. It develops vertically thin and horizontally extended ( $L_b \ll \ell_g$ ) pancake-like structures (e.g. Brethouwer et al. 2007). Its energy dissipation is also significantly different from that described by the Kolmogorov picture, as the vertical turn-over of its energy-containing eddies is strongly suppressed by the density stratification. In the ICM, a typical turbulence Froude number lies in the intermediate regime of  $Fr \sim O(1)$  (Shi et al. 2018, see also Fig. 2). How much would ICM turbulence evolution in this regime differ from that of homogeneous isotropic turbulence requires dedicated studies.

<sup>1</sup> Some clusters may have a very flat entropy profile  $d \ln K/dr \approx 0$  in the center and an associated drop of the Brunt-Väisälä frequency. However, this is usually limited to a very small radial range up to a few tens of kpc.

<sup>2</sup> What we define here is a Froude number for the whole turbulence velocity field, in contrast to the eddy Froude number which is defined for individual turbulence eddies.

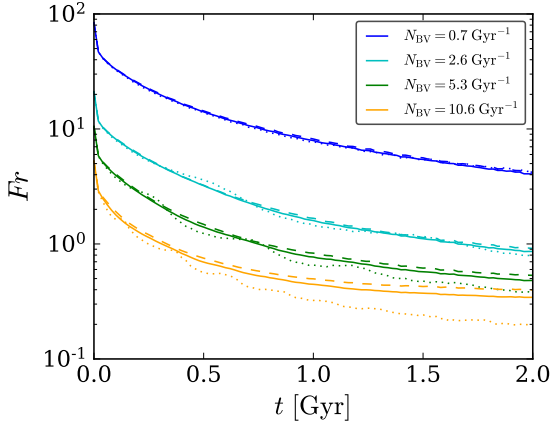


**Figure 2.** Time evolution of the turbulence Froude number (solid lines). The dashed lines show the scaled horizontal Froude number defined using horizontal turbulence velocity and energy-containing scale, whereas the dotted lines show the corresponding scaled vertical Froude number. Their deviation from the solid lines reflects the velocity anisotropy.

### 3 METHODS

In this study, we perform idealized hydrodynamical numerical simulations to examine the effect of density stratification on ICM turbulence evolution. We use the FLASH code [Fryxell et al. \(2000\)](#) to solve the hydrodynamics equations

$$\frac{\partial \rho}{\partial t} + \nabla \cdot (\rho \mathbf{v}) = 0 \quad (5)$$

and

$$\frac{\partial (\rho \mathbf{v})}{\partial t} + \nabla \cdot (\rho \mathbf{v} \mathbf{v}) = -\nabla P + \rho \mathbf{g} \quad (6)$$

for a polytropic gas in a stationary external gravitational field with a constant gravitational acceleration  $\mathbf{g}$  in the  $-z$  direction. We simulate local 3D boxes with  $L_x = L_y = 200$  kpc and  $L_z = 250$  kpc with a resolution of  $256 \times 256 \times 320$ , and for a duration of  $t_{\max} = 2$  Gyr. Reflective hydrostatic boundary conditions are applied to top and bottom boundaries, and periodic boundary conditions to the sides. We impose damping to the velocity fields near the top and bottom boundaries to reduce boundary effects, and will omit the 20 grid points near the top and bottom boundaries which are affected by the damping in the presentation below. This leaves a vertical domain size of  $L'_z = 218.75$  kpc.

The gas is chosen to have an exponential initial density profile  $\rho_0 = \bar{\rho} e^{-z/H_\rho}$  with a scale-height of

$$H_\rho = \frac{c_s^2}{\gamma g}, \quad (7)$$

where the gas adiabatic index  $\gamma = 5/3$  is relevant for fully ionised ICM, and the sound speed  $c_s$  is chosen to be a constant across the simulation domain. The corresponding initial pressure

$$P_0 = \frac{c_s^2 \rho_0}{\gamma}, \quad (8)$$

and  $\rho_0, g$  satisfy the hydrostatic equilibrium condition.

Our initial conditions are meant to mimic local ICM conditions in various regions. We perform four simulation runs (I-IV) with different values of gravitational acceleration  $g$ , corresponding to  $N_{\text{BV}} = 0.7 \text{ Gyr}^{-1}$ ,  $2.6 \text{ Gyr}^{-1}$ ,  $5.3 \text{ Gyr}^{-1}$  and  $10.6 \text{ Gyr}^{-1}$ , representing the cluster outskirts, intermediate regions, central regions

of non-cool-core clusters, and central regions of cool-core clusters, respectively (Fig. 1). We also include a simulation with no density stratification i.e.  $g = 0$  as a comparison.

We use an identical initial turbulence velocity field for all simulation runs to highlight the effect of density stratification on the subsequent evolution. The initial velocity field is generated using a zero mean Gaussian random field with an energy spectrum

$$E(k) \propto (k/k_c)^{-5/3} e^{-k_c/k}, \quad (9)$$

mimicking a 3D turbulence spectrum with a Kolmogorov  $k^{-5/3}$  inertial range and a large scale cutoff  $k_c = 0.24 \text{ kpc}^{-1}$ . This initial energy spectrum peaks at a length scale of  $2\pi\ell_g = 43.6$  kpc. We remove the compressive component to generate a solenoidal velocity field in correspondence to the subsonic nature of typical intracluster turbulence. Then we normalize the initial turbulence energy spectrum to have a velocity dispersion of  $\sigma_0 = 278 \text{ km/s}$  and an initial specific kinetic energy  $e_0 = \sigma_0^2/2$ . The resulting velocity field has several desired features e.g. statistically homogeneity and isotropy, the proper energy spectrum and the complex, three-dimensional structure expected of a turbulent flow field.

The physical evolution of such an initial velocity field is fully dictated by two dimensionless control parameters: the Froude number  $Fr$  which reflects the relative importance of the buoyancy force, and the Mach number  $\mathcal{M}$  which shows the compressibility of the gas and its ability to generate sound waves. In this study, we want to single out the buoyancy effect and thus work in the low Mach number limit by choosing an unphysical high background temperature  $T = 512 \text{ keV}$  to suppress the generation of sound waves. We focus on the range of Froude number from  $Fr \lesssim 1$  to  $Fr \sim 10$  relevant to galaxy clusters. The Froude number evolution of our four density-stratified simulations are presented in Fig. 2. We summarise the Froude number and the other domain-size related dimensionless parameters of our simulation runs in Table. 1.

## 4 RESULTS

### 4.1 Energy evolution

#### 4.1.1 Kinetic-potential energy conversion and power law asymptotes

For homogeneous, isotropic turbulence, the turbulence kinetic energy decays in a power law fashion

$$e_{\text{kin}}(t) = \frac{\sigma^2}{2} \propto t^{-n} \quad (10)$$

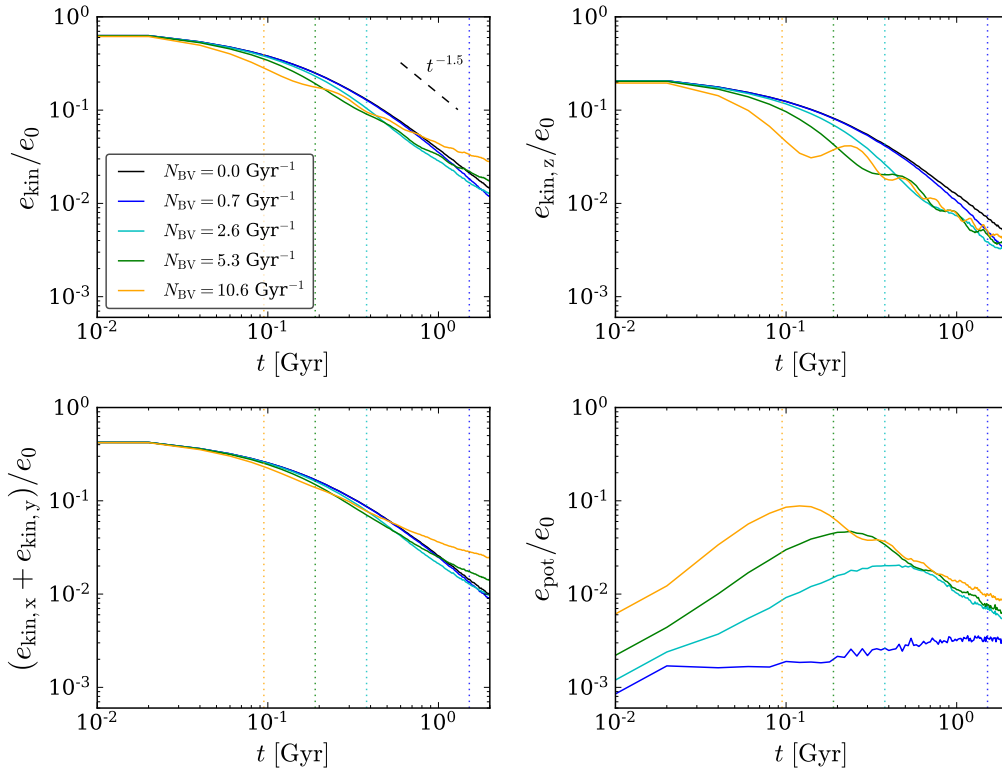
with an exponent  $n \approx 1.5$  (e.g. [Landau & Lifshitz 1959](#); [Frisch 1995](#); [Subramanian et al. 2006](#)).

Fig. 3 shows a comparison of the evolution of energy densities in our different simulation runs. Apparently, the turbulence kinetic energy evolution (top left panel) in a density-stratified medium (colored lines) differs from that in a homogeneous medium (black line) and shows much richer behavior. There are oscillations in the kinetic energy evolution in a density-stratified medium, and the logarithmic slope of the kinetic energy time evolution asymptotes to a value shallower than of  $n \approx -1.5$  for homogeneous turbulence. In the case of a high density stratification with  $N_{\text{BV}} = 10.6 \text{ Gyr}^{-1}$ , the logarithmic slope becomes as shallow as  $-0.7$ .

The oscillations in the kinetic energy evolution is created by a conversion between the vertical kinetic energy (top right panel)

**Table 1.** Dimensionless parameters of the simulations.

		Simulation runs			
		$N_{\text{BV}} [\text{Gyr}^{-1}]$			
		I	II	III	IV
		0.7	2.6	5.3	10.6
$Fr_i$	Initial Froude number	84.4	21.1	10.55	5.27
$Fr_{2\text{Gyr}}$	Froude number at 2 Gyr	4.1	0.86	0.48	0.34
$L_{b,i}/L'_z$	Initial buoyancy scale over vertical domain size	12	3.1	1.5	0.77
$L_{b,2\text{Gyr}}/L'_z$	Buoyancy scale at 2 Gyr over vertical domain size	1.3	0.35	0.21	0.13
$H_\rho/L'_z$	Density scale height over vertical domain size	53	13	6.5	3.2


**Figure 3.** Comparison of turbulence energy evolution in media with different density stratification. Shown are the time evolution of the average turbulence kinetic energy (top left panel), its vertical (top right panel) and horizontal (bottom left panel) components, and the fluctuation gravitational potential energy (bottom right panel) of the simulation runs with different Brunt-Vaisälä frequencies (colored lines) in comparison to those in a homogeneous isotropic medium (black lines).

and the fluctuation potential energy (bottom right panel)

$$e_{\text{pot}} = -\frac{1}{2} \frac{g}{\rho_0} \left( \frac{d\rho}{dz} \right)^{-1} \overline{\delta\rho^2}, \quad (11)$$

as a result of the buoyancy induced by density stratification. Here,  $\delta\rho = \rho - \rho_0$  is the density fluctuation. As shown by Fig. 5, this energy conversion leaves both the vertical kinetic energy (blue dashed line) and the potential energy (magenta dotted line) oscillate at opposite phases.

The time scale of this energy conversion is well captured by the typical buoyancy time  $1/N_{\text{BV}}$  (vertical dotted lines). As shown by Fig. 4, the peak of the fluctuation potential energy occurs at a time  $t \approx 1.2/N_{\text{BV}}$ , and both the vertical kinetic energy and the fluctuation potential energy asymptote to a power-law evolution after the first period of the oscillation at  $t \gtrsim 1/N_{\text{BV}}$ . The long term asymptotes show roughly universal shapes:

$$e_{\text{kin},z}/e_0 \propto N_{\text{BV}}(N_{\text{BV}}t)^{-1.2} \quad (12)$$

and

$$e_{\text{pot}}/e_0 \propto N_{\text{BV}}(N_{\text{BV}}t)^{-0.9}, \quad (13)$$

if we neglect the low stratification run which has low signal to noise. This shows that (1) the long term decay of the vertical kinetic energy and the fluctuation potential energy is governed by how many buoyancy periods the system has evolved; (2) the power-law slopes are different, and both shallower than  $-1.5$ ; (3) their asymptotic amplitudes at the same time  $t$  depends little on  $N_{\text{BV}}$ , and thus the amplitude at the same buoyancy period  $N_{\text{BV}}t$  are roughly proportional to  $N_{\text{BV}}$ ; and (4) the amplitude of the potential energy is greater than that of the vertical kinetic energy (see also Fig. 5 for a comparison of energy amplitudes for individual simulations).

Another consequence of this vertical energy conversion is the emergence of velocity anisotropy. The more stratified the background density is, the more anisotropic the turbulence kinetic energy becomes, as reflected by the greater separation between the

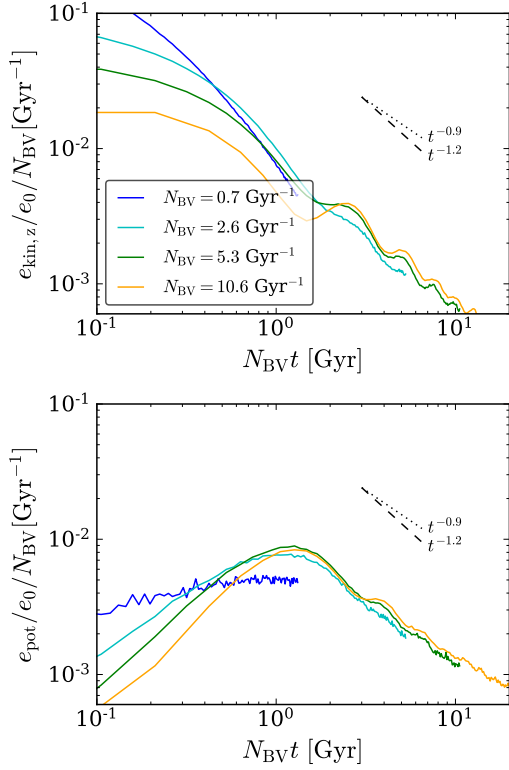


**Figure 4.** Right panels of Fig. 3 plotted with scaled axes showing universal behavior at long times ( $N_{BV}t > 1$ ).

vertical and horizontal turbulence kinetic energies (Fig. 5). At long times, it is the horizontal component (bottom left panel of Fig. 3) that contributes more to the total kinetic energy, since density stratification suppresses turbulence eddy turn-over in the vertical direction especially for the large energy-containing eddies. Consequently, the kinetic energy of these large horizontal eddies can hardly cascade to smaller scales and get dissipated, similar to the case in 2D turbulence. The same suppression effect also results in the dominance of large eddies in the horizontal plane, which will be shown in Sect. 4.2.

#### 4.1.2 Radial dependence of ICM turbulence

Let simulations with different density stratification represent different regions of the ICM, the dependence of turbulence energy evolution on density stratification then implies a radial-dependence of ICM turbulence.

As shown by Fig. 3, in the first few hundred million years after the injection of turbulence, the turbulence kinetic energy is smaller where the density stratification is higher (top left panel), because a greater part of its vertical component (top right panel) is converted into fluctuation potential energy (bottom right panel). However, at later times turbulence kinetic energy is actually larger where the density stratification is higher, as shown by the reversed order of the colored lines in the top left panel at  $t \gtrsim 0.5$  Gyr. This is the result of two factors. First, in the vertical direction, some of the energy stored as fluctuation potential energy flows back to kinetic energy, and at long times the vertical kinetic energy is rather independent of the density stratification (upper right panel). Second, turbulence

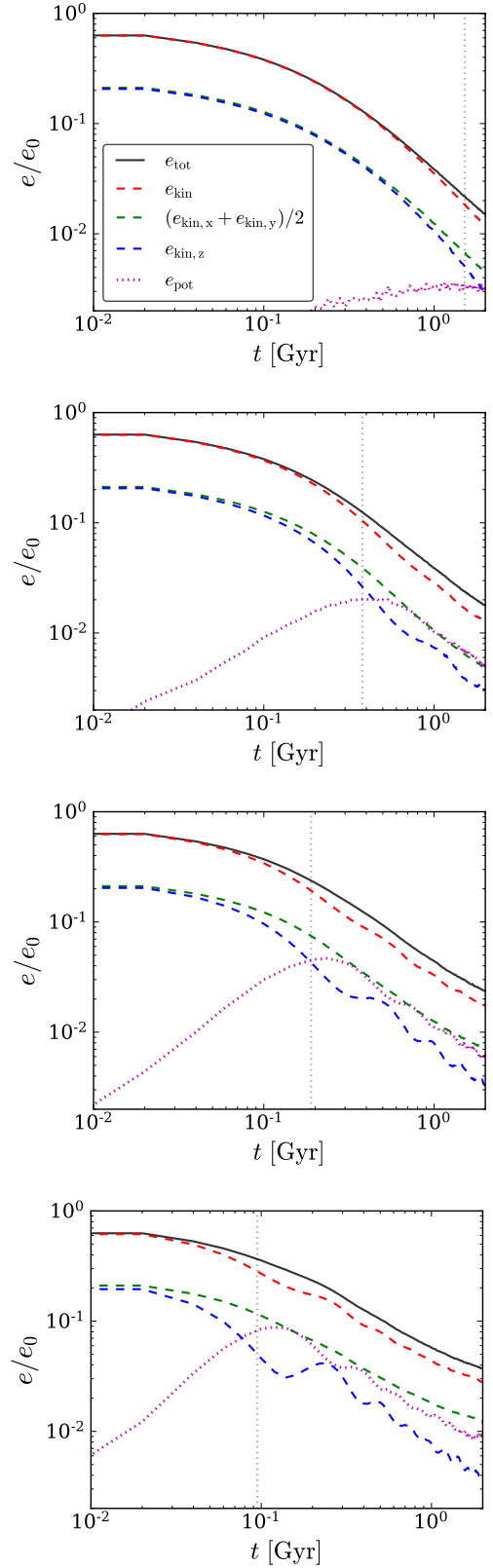


**Figure 5.** Evolution of the energy densities for simulations with different density stratification (different panels). The vertical dashed line in each panel marks the Brunt-Väisälä time  $1/N_{BV}$  in the corresponding simulation. The red dashed line and the magenta dotted line mark the time evolution of turbulence kinetic energy and the fluctuation potential energy respectively, and the black line is the sum of the two. The green/ blue dashed lines represent the 1D horizontal/ vertical turbulence kinetic energy.

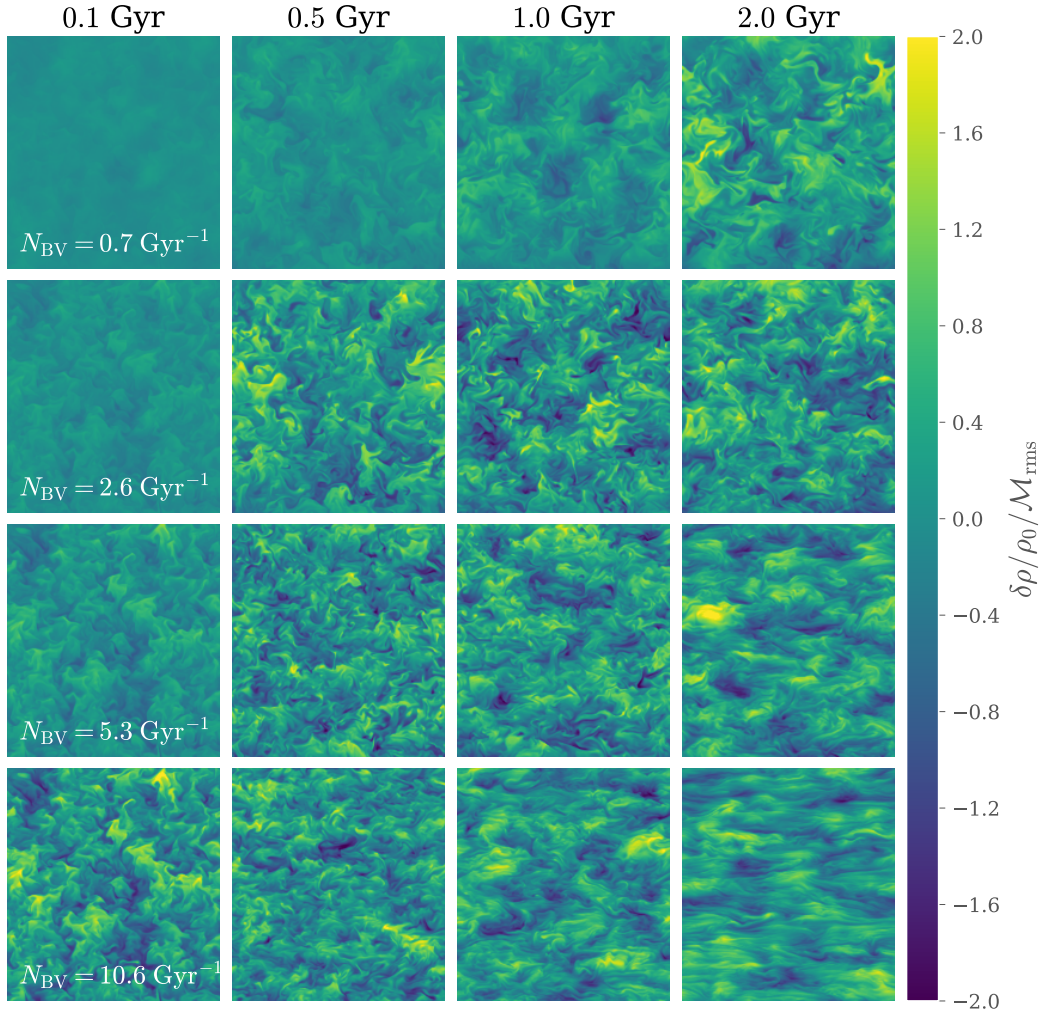


**Figure 6.** Vertical 200 kpc  $\times$  218.75 kpc slices of density fluctuation evolution through the mid-plane of the x-axis for the simulation runs I-IV with various density gradients (rows) at four various times (columns) after turbulence injection at  $t = 0$ .

evolving in a more density-stratified medium manages to keep more horizontal kinetic energy at long times (bottom left panel).

This time reversal of the turbulence radial dependence is not found in the Shi et al. (2018) detailed analysis of ICM turbulence decay in two galaxy clusters selected from a set of cosmological numerical simulations. In both clusters studied by Shi et al. (2018), a faster turbulence decay at small radii following injection by major mergers leads to an increasing turbulence amplitude with cluster radius, and this positive radial dependence stays even after a few Gyrs' evolution. Statistical results of cosmological numerical simulations (e.g. Lau et al. 2009; Battaglia et al. 2012; Nelson et al. 2014) also support a positive radial dependence of turbulence being the generic state of ICM. This apparent discrepancy is likely explained by the neglect of the background density and gravitational potential variations in the current study, as will be discussed in Sect. 5.

## 4.2 Morphology

Figs. 6 and 7 show the turbulence morphological evolution as traced by the density fluctuation for the four simulation runs

representing different regions of the ICM. Two signs of density-stratification influence are clear in the central regions of galaxy clusters (simulation runs with  $N_{BV} = 5.3$  and  $10.6 \text{ Gyr}^{-1}$ ) at late times: the loss of statistical isotropy in the vertical plane (Fig. 6), and the dominance of large eddies in the horizontal plane (Fig. 7).

The degree of density-stratification influence is well-described by the buoyancy period  $N_{BV}t$  or the Froude number (Fig. 2), with  $N_{BV}t \gtrsim 5$  and  $Fr \lesssim 1$  marking the regime where the influence on morphology is apparent. In an extreme case in the ICM where a cool-core is left quiescent for  $t \approx 2 \text{ Gyr}$  i.e. since redshift  $\approx 0.2$  (bottom right panel), the Froude number reaches as low as  $Fr \approx 0.3$ , and a clear layered structure with thickness  $L_b < \ell_g$  develops. The velocity anisotropy and density fluctuation associated with this layered structure are in principle observable from X-ray line profile and surface brightness fluctuation, albeit challenging due to their small amplitude.

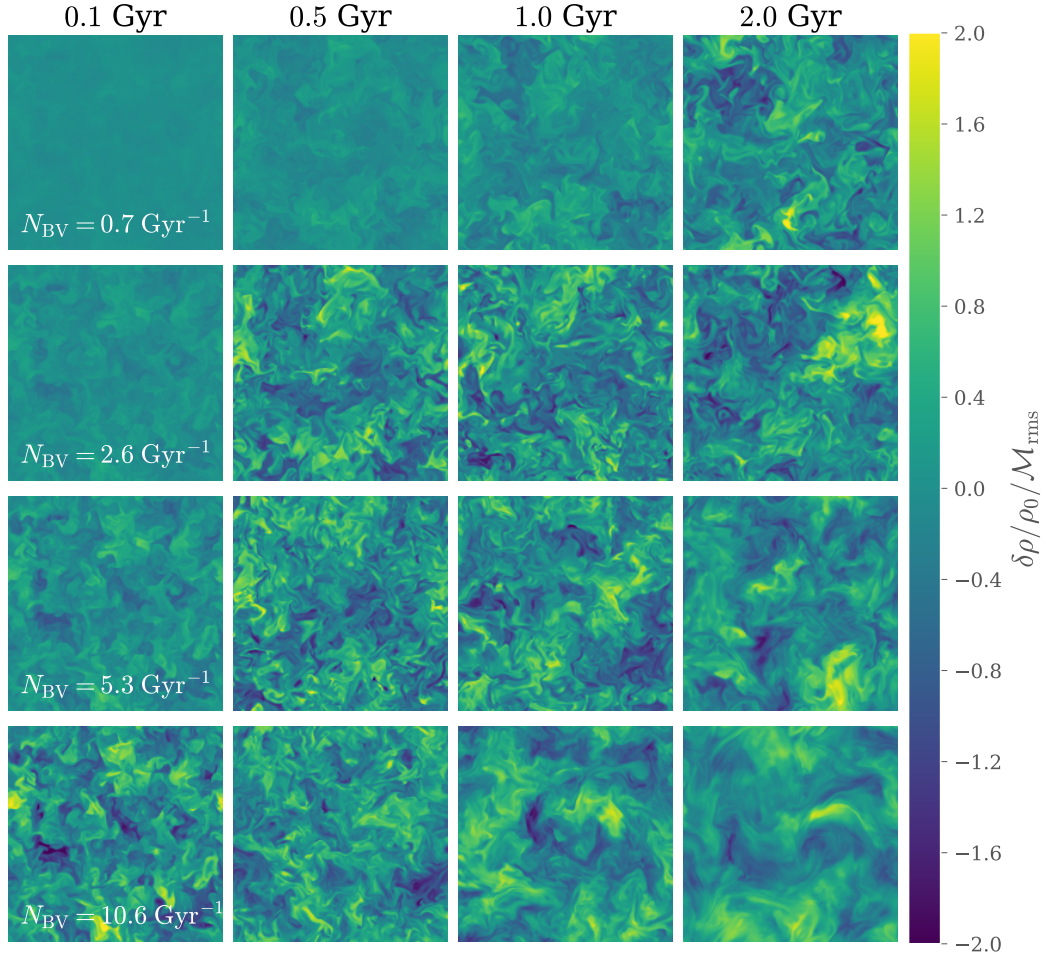


Figure 7. Same as Fig. 6, but for horizontal 200 kpc  $\times$  200 kpc slices through the mid-plane of the z-axis.

### 4.3 Density fluctuation - Mach number relation in the stratified ICM

Density fluctuations in the ICM are in general associated with ICM motions. There have been attempts to infer the latter using X-ray observations of the density fluctuations (Schuecker et al. 2004; Churazov et al. 2012; Walker et al. 2015; Zhuravleva et al. 2018), which would rely on a correct theoretical understanding of the relation between the two quantities.

In a homogeneous, isotropic turbulent medium, the amplitude of density fluctuations depends predominantly on the r.m.s. turbulence Mach number  $\mathcal{M}_{\text{rms}}$  and the associated compressibility of the velocity field. For a qualitative understanding of this dependence, it is most convenient to observe the equation of motion for the gas Eq. 6. The divergence of Eq. 6 leads to the pressure Poisson equation in the form of (e.g. Landau & Lifshitz 1959)

$$\nabla^2 P = -(\nabla \mathbf{v})^T : \nabla \mathbf{v} \quad (14)$$

when the motions are solenoidal i.e.  $\nabla \cdot \mathbf{v} = 0$  and the medium is incompressible. The first order term in velocity on the l.h.s. of Eq. 6 does not enter due to the assumption of solenoidal motions, and the lowest order dependence of gas pressure or density on velocity is quadratic. Thus, when the turbulence is driven with solenoidal modes, as the compressible modes do not develop in the low Mach

number limit  $\mathcal{M}_{\text{rms}} \ll 1$ , the r.m.s. density fluctuation  $\langle \delta \rho / \rho \rangle_{\text{rms}}$  scales as  $\mathcal{M}_{\text{rms}}^2$  at the lowest order. At a finite Mach number, the compressible modes including sound waves are excited, the first order term in velocity in the equation of motion starts to gain dominance, leading to a linear increase of the density fluctuation with  $\mathcal{M}_{\text{rms}}$ , and thus a flattening in the density fluctuation - turbulence Mach number scaling (see also Pan & Scannapieco 2010; Mohapatra & Sharma 2019). This trend continues to the supersonic regime, and the scaling approaches a logarithmic form (Molina et al. 2012) in the high Mach number limit where the velocity field is dominated by shock waves.

Even a moderate density stratification alters the relation completely. In a density-stratified medium, the buoyancy-induced  $\langle \delta \rho / \rho \rangle_{\text{rms}}$  scales linearly with  $\mathcal{M}_{\text{rms}}$ , even in the low Mach number limit (Eq. 4 in Zhuravleva et al. 2014). Other effects such as perturbations of the gravitational potential and thermal conduction (Churazov et al. 2012; Gaspari & Churazov 2013; Gaspari et al. 2014) also affect the relation (see discussion session).

Our simulations present a case study of the density fluctuation - velocity connection in the low Mach number regime that is induced by buoyancy alone. We note two facts that are often neglected in the literature. First, in a non-equilibrium system like the ICM in a growing galaxy cluster, the coefficient in the linear re-

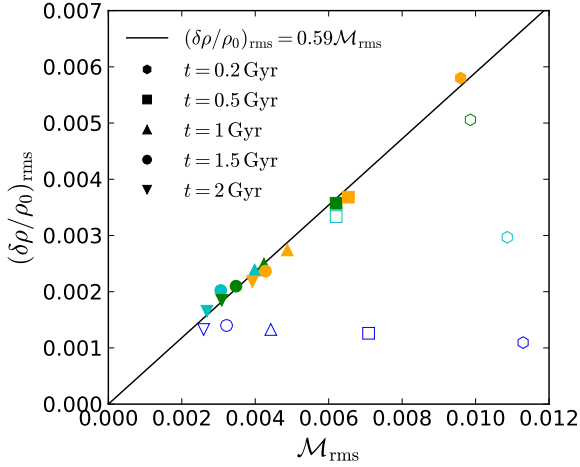


**Figure 8.** Density fluctuation - Mach number relation in the energy equipartition regime. The blue, cyan, green and orange colors indicate simulation runs with  $N_{\text{BV}} = 0.7, 2.6, 5.3$  and  $10.6 \text{ Gyr}^{-1}$  respectively. Different markers show snapshots at  $t = 0.2, 0.5, 1, 1.5$  and  $2 \text{ Gyr}$ . Snapshots that have obtained saturated energy ratios (with  $t > 2/N_{\text{BV}}$ ) are plotted in filled markers, whereas those which have not are plotted in open markers.

lation between  $\langle \delta\rho/\rho \rangle_{\text{rms}}$  and  $M_{\text{rms}}$  is in general a time variable, and it also depends on the density stratification and thus cluster radius, as shown by Figs. 3 and 5 (note that  $e_{\text{pot}} \propto \langle \delta\rho/\rho \rangle_{\text{rms}}^2$  and  $e_{\text{kin}} \propto M_{\text{rms}}^2$ ). Only when the system is allowed to relax for a relatively long time ( $t \gtrsim 1/N_{\text{BV}}$ ) and also in the absence of significant changes of the gravitational potential, the coefficient saturates to a nearly constant value presented in Fig. 8. Second, the linear relation holds only on a scale much larger than  $\max(\ell_g, L_b)$ . As shown by Fig. 9, there is no local correspondence between the density fluctuation and the amplitude of turbulence velocity. This can be understood by recalling the fact that the former is a passive scalar tracer of the latter. The morphology of the density field keeps a memory of the velocity field in the past.

## 5 DISCUSSIONS

### 5.1 Global variations of gas density and gravitational potential

In our study, we have examined turbulence decay in a stable medium where the background gravitational potential and gas density stay fixed throughout the evolution. In reality, the merger events that inject turbulence into the ICM would also trigger variations of the gas density and the gravitational potential. These variations will couple to the turbulence decay process and alter our results on turbulence energy evolution presented in Sect. 4.1, which we will discuss below.

We consider here the turbulence evolution after a head-on major merger event which, when present, dominates ICM turbulence injection (Paul et al. 2011; Nelson et al. 2012). Especially, we focus on the evolution following the core collision which marks the time of most intensive turbulence injection (Shi et al. 2018). As is shown in Shi et al. (2018), there is a fast decay phase lasting for about 1 Gyr starting from the core collision, during which the gravitational potential rapidly flattens as the dark matter halos of the merging ob-

jects pass through and move away from each other, and the merged ICM rapidly expands.

In the presence of density stratification, a rapid flattening of gravitational potential after a major merger event would channel away the gravitational potential energy associated with density fluctuations. The shortage of potential energy would then forge more conversion of turbulence kinetic energy into potential energy. Therefore, instead of reaching a balanced state where both energies decay in power-law fashion as shown in Figs. 3, 4 and 5, a fast channel of turbulence kinetic energy loss would be formed in the system in comparison to the regular turbulence cascade. The time scale for this fast energy loss is characterized by that of the kinetic-potential energy conversion i.e. the buoyancy time  $1/N_{\text{BV}}$ . This mechanism may help the inner regions with stronger density stratification maintain a lower level of turbulence kinetic energy for  $\sim \text{Gyr}$  time before the final reversal of the radial dependence when the residue trapped horizontal vortical modes gain dominance. Considering that turbulence injection by merger events is in general frequent in the ICM, and that each injection is also extended in time (e.g. Zhang et al. 2016), this final reversal may never be reached. Thus, in this scenario, an increasing turbulence amplitude with radius is the generic state of the ICM, in accordance with the previous numerical results of ICM turbulence (Lau et al. 2009; Battaglia et al. 2012; Nelson et al. 2014; Shi et al. 2018).

At the same time, a rapid expansion of the ICM following a major merger event will directly cause adiabatic cooling of both the thermal and the kinetic components of the ICM (Robertson & Goldreich 2012), which also means a fast decay channel of the ICM turbulence. In contrast to the mechanism caused by gravitational potential flattening, this mechanism does not depend on ICM density stratification. Nevertheless, it can introduce a radial dependence if the degree of ICM density expansion is radial dependent.

The above discussion has not considered the role of bulk motions in the energy flow, which can be important when the gas cores of the progenitors are not destroyed in the merger. It also neglects secondary effects such as the variation of the Brunt-Väisälä frequency due to the flattening of gravitational potential and the evolution of the entropy profile. Also, the relative importance of the gravitational potential flattening effect and the ICM expansion effect to the ICM turbulence evolution is not clear. All these would require further systematic studies with more realistic numerical simulations. Nevertheless, one hint is presented in the case study of Shi et al. 2018 (see their Fig. 6). There, the time evolution of the ICM velocity fields after a major merger is found to resemble that of the gravitational potential rather than the gas density, suggesting a direct interaction between gravity and turbulence and the dominance of the gravitational potential flattening effect.

### 5.2 Thermal conduction

Thermal conduction, which we neglect in this paper, can potentially influence the dynamics of the ICM and particularly the evolution of ICM turbulence. If thermal conduction is efficient, the characteristic frequency of buoyant oscillations is not described by the Brunt-Väisälä frequency as defined in Eq. 1 but with the entropy gradient in Eq. 1 replaced by the temperature gradient (e.g. Ruszkowski & Oh 2011), reducing the efficiency of turbulent kinetic energy - gravitational potential energy conversion, and consequently reducing the buoyancy-induced density fluctuations in the ICM (Gaspary et al. 2014).

Turbulence, on the other hand, plays an important role in determining the potency of ICM thermal conduction by re-orienting

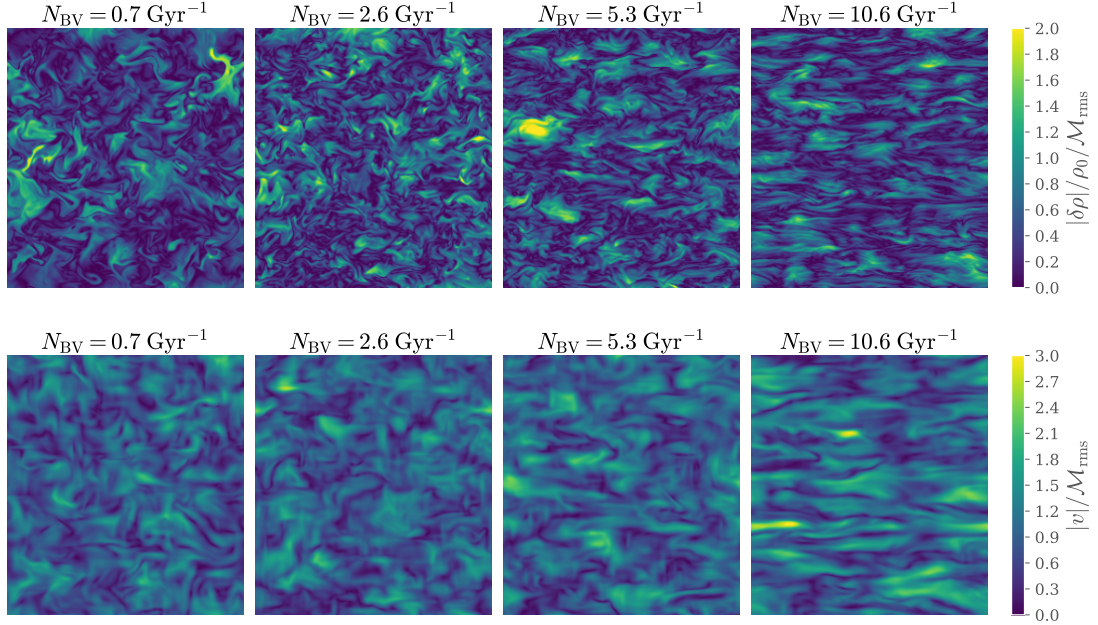


**Figure 9.** Vertical slices of density fluctuation (upper panels) and velocity magnitude (lower panel) at  $t = 2$  Gyr.

and amplifying ICM magnetic fields, with the latter suppressing ICM thermal conductivity compared to its un-magnetized Spitzer value. Due to the complex interplay between ICM thermal conduction, turbulence, magnetic fields and buoyancy, the efficiency of thermal conduction in the ICM remains highly uncertain. However, recent studies of both microscopic physics (e.g. Komarov et al. 2016, 2018; Roberg-Clark et al. 2018) and macroscopic ICM structural stability (e.g. Fang et al. 2018) suggest that the effective thermal conductivity in the ICM may be very small.

## 6 CONCLUSIONS

We have explored how the density stratification in the intracluster medium affects the ICM turbulence time evolution, morphology, and the induced density fluctuations with the aid of 3D hydrodynamic simulations. In particular, we examine if the Brunt-Väisälä buoyancy frequency, which decreases by at least an order of magnitude from the central region of a galaxy cluster to its virial radius, would introduce a radial dependence to the ICM turbulence evolution. The main results are as follows.

- *The Froude number of ICM turbulence*

ICM turbulence is typically mildly-stratified with a Froude number  $Fr \sim O(1)$ . In the central region, the Froude number can reach as low as  $Fr \sim O(0.1)$ , which is still larger than the condition  $Fr < 0.1$  commonly used to identify strongly-stratified turbulence. However, as we have shown in this paper, the energy evolution, morphology and density fluctuation of ICM turbulence with such a range of Froude number already show a qualitative difference from those of homogeneous, isotropic turbulence.

- *Energy evolution of ICM turbulence*

The time evolution of turbulence energy in the density-stratified ICM deviates from that in a homogeneous, isotropic medium.

The buoyancy effect of a density stratification lets turbulence generate density fluctuations, converting part of its vertical kinetic energy to fluctuation potential energy and back on a time scale of the buoyancy time  $1/N_{BV}$ . When the gravitational potential is kept constant, the kinetic and potential energies approach a balanced state at long times ( $t \gtrsim 1/N_{BV}$ ), where both evolve in a power-law fashion with a slope shallower than the  $n \approx -1.5$  slope for homogeneous isotropic turbulence. We speculate that when the rapid flattening of gravitational potential following a major merger event is taken into account, the conversion between the two energies becomes one-way: turbulence kinetic energy converts quickly (with a time scale of  $1/N_{BV}$ ) into potential energy, which keeps decreasing with the flattening of the gravitational potential.

- *Radial dependence of ICM turbulence*

In the more stratified central regions of the ICM, there is a faster initial conversion from the injected turbulence kinetic energy to the potential energy, resulting in an increasing turbulence amplitude with cluster radius for  $t \approx 0.2$  Gyr. In our simulations where the gravitational potential is kept constant, this radial dependence will be reversed later on due to a backflow of potential energy to vertical turbulence kinetic energy, plus the trapping of more horizontal turbulence kinetic energy as a consequence of suppression of vertical eddy turn-over in the more density-stratified central regions. The inclusion of gravitational potential flattening may help maintain the positive dependence of turbulence amplitude on cluster radius for a longer time ( $t \sim$  Gyr), during which turbulence kinetic energy decays at a time scale characterized by the buoyancy time  $1/N_{BV}$ . This is potentially the underlying physics for the faster turbulence decay in the inner ICM regions discovered by Shi et al. (2018), and that for the increasing turbulence amplitude observed in cosmological numerical simulations.

- *ICM turbulence morphology*

ICM velocity field is in general morphologically isotropic. How-

ever, in the case of turbulence in a cool core which has been quiescent for at least  $\sim$  Gyr, the Froude number reaches as low as  $Fr \sim 0.3$ . In such a case, a clear density stratification influenced morphology – that of layered pancakes (vertically thin, horizontally large vortical eddies) develops for the turbulence velocity field and the density fluctuation it induces. The corresponding velocity anisotropy and the layered density fluctuations are in principle detectable through X-ray observations.

- *Density fluctuation - Mach number relation*

A linear relation holds between the r.m.s. density fluctuation and the r.m.s. turbulence Mach number in a density-stratified medium even in the low Mach number limit, but only when the quantities are averaged over a scale much larger than both the turbulence eddy size and the buoyancy scale. We find that the coefficient in the linear relation is in general a variable with radius and time, which saturates to a constant only when the system is allowed to relax for a relatively long time  $t \gtrsim 1/N_{\text{BV}}$ , and when the gravitational potential is not significantly changing with time.

## ACKNOWLEDGEMENTS

The software used in this work was in part developed by the DOE NNSA-ASC OASCR Flash Center at the University of Chicago.

## REFERENCES

- Battaglia N., Bond J. R., Pfrommer C., Sievers J. L., 2012, *ApJ*, **758**, 74
- Bonafede A., Feretti L., Murgia M., Govoni F., Giovannini G., Dallacasa D., Dolag K., Taylor G. B., 2010, *A&A*, **513**, A30
- Brethouwer G., Billant P., Lindborg E., Chomaz J.-M., 2007, *Journal of Fluid Mechanics*, **585**, 343
- Churazov E., Forman W., Jones C., Sunyaev R., Böhringer H., 2004, *MNRAS*, **347**, 29
- Churazov E., et al., 2012, *MNRAS*, **421**, 1123
- Fang X.-E., Guo F., Yuan Y.-F., Mou G., 2018, *ApJ*, **863**, 177
- Frisch U., 1995, *Turbulence. The legacy of A. N. Kolmogorov*. Cambridge University Press, Cambridge. Cambridge University Press
- Fryxell B., et al., 2000, *ApJS*, **131**, 273
- Gaspari M., Churazov E., 2013, *A&A*, **559**, A78
- Gaspari M., Churazov E., Nagai D., Lau E. T., Zhuravleva I., 2014, *A&A*, **569**, A67
- Hitomi Collaboration et al., 2016, *Nature*, **535**, 117
- Hitomi Collaboration et al., 2018, *Publications of the Astronomical Society of Japan*, **70**, 10
- Hopfinger E. J., 1987, *Journal of Geophysical Research*, **92**, 5287
- Iapichino L., Niemeyer J. C., 2008, *MNRAS*, **388**, 1089
- Khatri R., Gaspari M., 2016, *MNRAS*, **463**, 655
- Komarov S. V., Churazov E. M., Kunz M. W., Schekochihin A. A., 2016, *MNRAS*, **460**, 467
- Komarov S., Schekochihin A. A., Churazov E., Spitkovsky A., 2018, *Journal of Plasma Physics*, **84**, 905840305
- Komatsu E., Seljak U., 2001, *MNRAS*, **327**, 1353
- Landau L. D., Lifshitz E. M., 1959, *Fluid Mechanics*. Pergamon Press, Oxford. Oxford: Pergamon Press
- Lau E. T., Kravtsov A. V., Nagai D., 2009, *ApJ*, **705**, 1129
- Miniati F., 2014, *ApJ*, **782**, 21
- Miniati F., Beresnyak A., 2015, *Nature*, **523**, 59
- Mohapatra R., Sharma P., 2019, *MNRAS*, **484**, 4881
- Molina F. Z., Glover S. C. O., Federrath C., Klessen R. S., 2012, *MNRAS*, **423**, 2680
- Murgia M., Govoni F., Feretti L., Giovannini G., Dallacasa D., Fanti R., Taylor G. B., Dolag K., 2004, *A&A*, **424**, 429
- Navarro J. F., Frenk C. S., White S. D. M., 1996, *ApJ*, **462**, 563
- Nelson K., Rudd D. H., Shaw L., Nagai D., 2012, *ApJ*, **751**, 121
- Nelson K., Lau E. T., Nagai D., 2014, *ApJ*, **792**, 25
- Norman M. L., Bryan G. L., 1999, in Roeser H.-J., Meisenheimer K., eds, *Lecture Notes in Physics*, Berlin Springer Verlag Vol. 530, The Radio Galaxy Messier 87. p. 106 ([arXiv:astro-ph/9802335](https://arxiv.org/abs/astro-ph/9802335)), [doi:10.1007/BFb0106425](https://doi.org/10.1007/BFb0106425)
- Ozmidov R. V., 1965, *Atmos. Oceanic Phys.*, **1**, 861
- Pan L. B., Scannapieco E., 2010, *The Astrophysical Journal*, **721**, 1765
- Paul S., Iapichino L., Miniati F., Bagchi J., Mannheim K., 2011, *ApJ*, **726**, 17
- Riley J. J., deBruynKops S. M., 2003, *Physics of Fluids*, **15**, 2047
- Roberg-Clark G. T., Drake J. F., Swisdak M., Reynolds C. S., 2018, *ApJ*, **867**, 154
- Robertson B., Goldreich P., 2012, *ApJ*, **750**, L31
- Ruszkowski M., Oh S. P., 2011, *MNRAS*, **414**, 1493
- Schuecker P., Finoguenov A., Miniati F., Böhringer H., Briel U. G., 2004, *A&A*, **426**, 387
- Shi X., Komatsu E. S., 2014, *MNRAS*, **442**, 521
- Shi X., Komatsu E., Nelson K., Nagai D. S., 2015, *MNRAS*, **448**, 1020
- Shi X., Komatsu E., Nagai D., Lau E. T., 2016, *MNRAS*, **455**, 2936
- Shi X., Nagai D., Lau E. T., 2018, *MNRAS*, **481**, 1075
- Simionescu A., et al., 2019, *Space Sci. Rev.*, **215**, 24
- Stillinger D. C., Helland K. N., Van Atta C. W., 1983, *Journal of Fluid Mechanics*, **131**, 91122
- Subramanian K., Shukurov A., Haugen N. E. L., 2006, *MNRAS*, **366**, 1437
- Vacca V., Murgia M., Govoni F., Feretti L., Giovannini G., Orrù E., Bonafede A., 2010, *A&A*, **514**, A71
- Vacca V., Murgia M., Govoni F., Feretti L., Giovannini G., Perley R. A., Taylor G. B., 2012, *A&A*, **540**, A38
- Vazza F., Brunetti G., Kritsuk A., Wagner R., Gheller C., Norman M., 2009, *A&A*, **504**, 33
- Vazza F., Jones T. W., Brueggen M., Brunetti G., Gheller C., Porter D., Ryu D., 2017, *MNRAS*, **464**, 210
- Vogt C., Enßlin T. A., 2005, *A&A*, **434**, 67
- Walker S. A., Sanders J. S., Fabian A. C., 2015, *MNRAS*, **453**, 3699
- Zhang C., Yu Q., Lu Y., 2016, *ApJ*, **820**, 85
- Zhuravleva I., et al., 2013, *MNRAS*, **435**, 3111
- Zhuravleva I., et al., 2014, *ApJ*, **788**, L13
- Zhuravleva I., Allen S. W., Mantz A., Werner N., 2018, *ApJ*, **865**, 53